MIT Libraries | DSpace@MIT

MIT Open Access Articles

Assessing the Influence of Secondary Organic versus Primary Carbonaceous Aerosols on Long-Range Atmospheric Polycyclic Aromatic Hydrocarbon Transport

Massachusetts Institute of Technology

Assessing the influence of secondary organic versus primary carbonaceous aerosols on long-range atmospheric PAH transport

C. L. Friedman[1], J. R. Pierce[2], and N. E. Selin[3]

[1] Center for Global Change Science and Leading Technology and Policy Initiative, Massachusetts Institute of Technology, Cambridge, Massachusetts
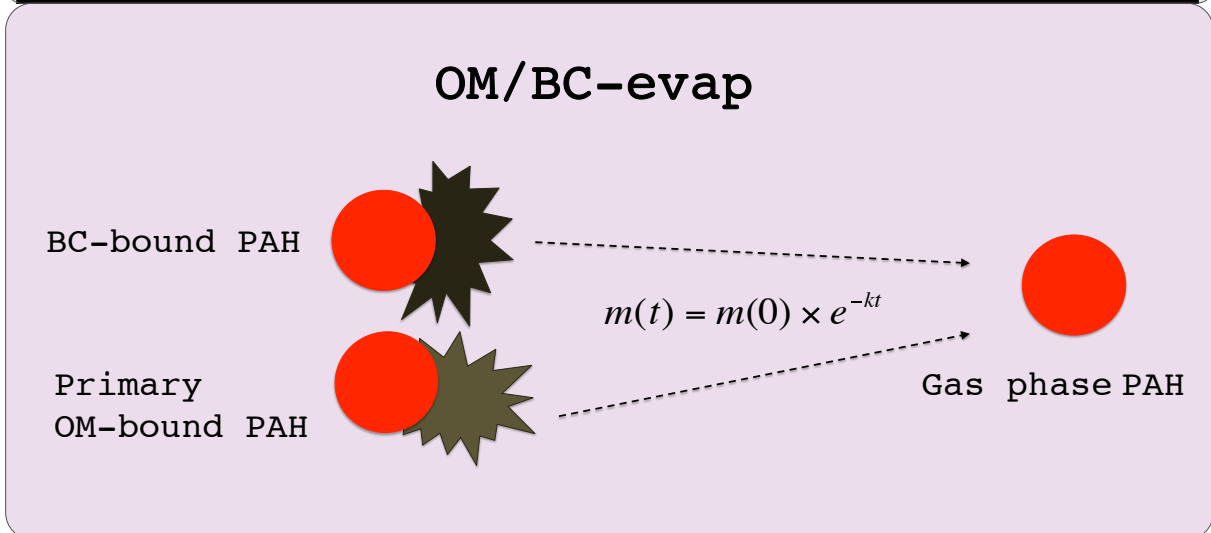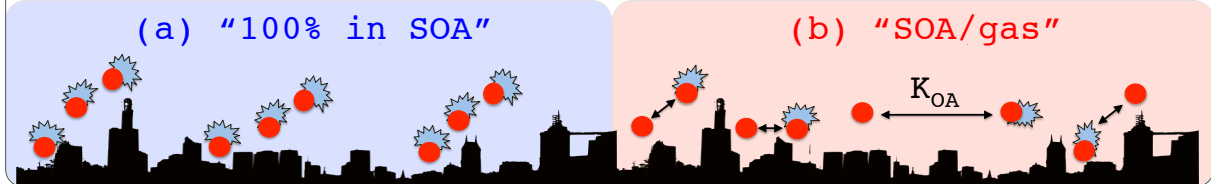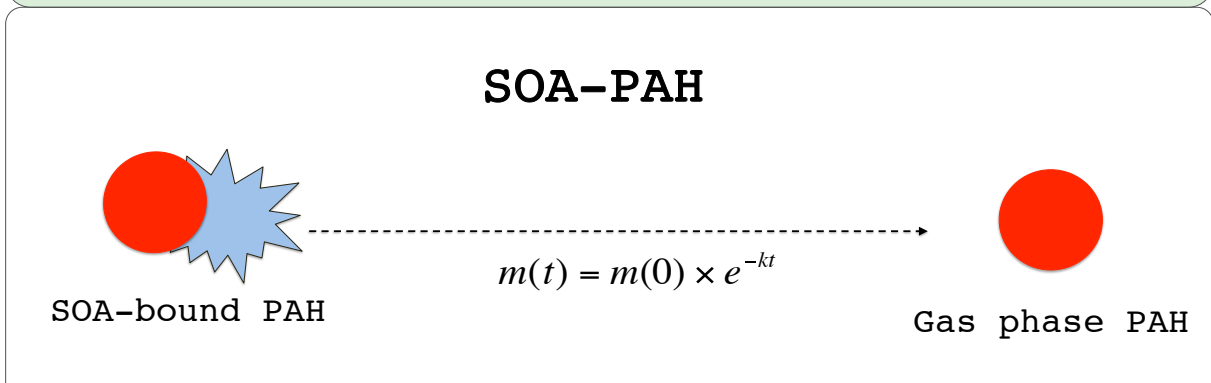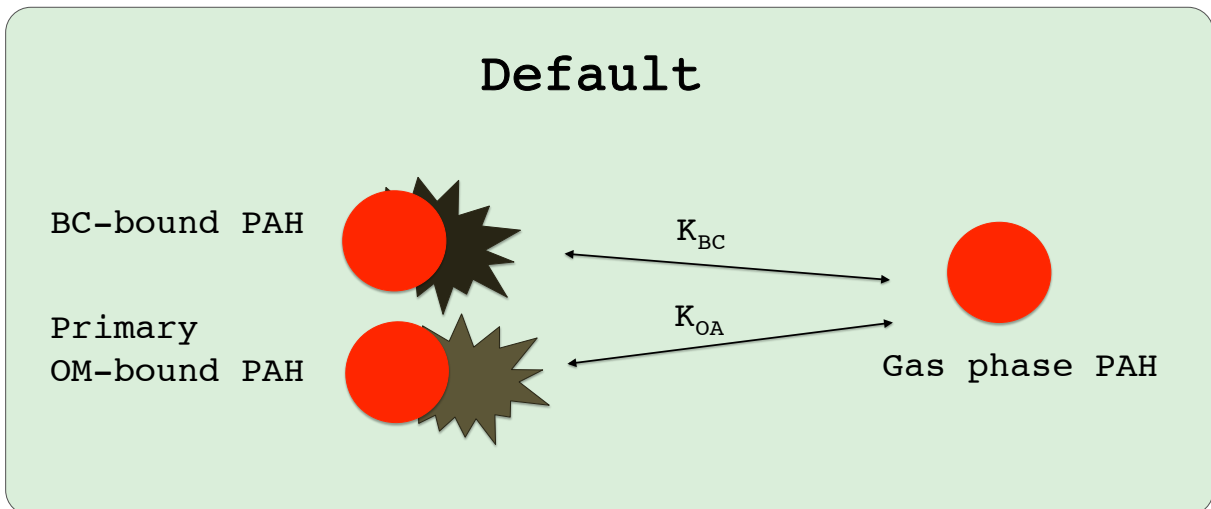
[2] Department of Atmospheric Science, Colorado State University, Fort Collins, Colorado

[3] Engineering Systems Division and Department of Earth, Atmospheric, and Planetary Science, Massachusetts Institute of Technology, Cambridge, Massachusetts

Correspondence to: C. L. Friedman (clf@mit.edu), Telephone: 617-324-2592, Fax: 617-253-7492

TOC Art

Abstract

We use the chemical transport model GEOS-Chem to evaluate the hypothesis that atmospheric polycyclic aromatic hydrocarbons (PAHs) are trapped in secondary organic aerosol (SOA) as it forms. We test the ability of three different partitioning configurations within the model to reproduce observed total concentrations in the mid-latitudes and the Arctic as well as mid-latitude gas-particle phase distributions. The configurations tested are: (1) the GEOS-Chem default configuration, which uses instantaneous equilibrium partitioning to divide PAHs between the gas phase, a primary organic matter (OM) phase (absorptive), and a black carbon (BC) phase (adsorptive); (2) an SOA configuration, in which PAHs are trapped in SOA when emitted and slowly evaporate from SOA thereafter, and (3) a configuration in which PAHs are trapped in primary OM/BC upon emission and subsequently slowly evaporate. We also test the influence of changing the fraction of PAH available for particle-phase oxidation. Trapping PAHs in SOA particles upon formation and protecting against particle-phase oxidation (2) better simulates observed remote concentrations compared to our default configuration (1). However, simulating adsorptive partitioning to BC is required to reproduce the magnitude and seasonal pattern of gas-particle phase distributions. Thus, the last configuration (3) results in the best agreement between observed and simulated concentration/phase distribution data. The importance of BC rather than SOA to PAH transport is consistent with strong observational evidence that PAH and BC are co-emitted.

Introduction

Polycyclic aromatic hydrocarbons (PAHs) are toxic semi-volatile organic compounds (SVOCs) that partition between gas and aerosol phases and travel long distances in the atmosphere.[1,2] The chemical and physical processes influencing transport of PAHs from areas of high emissions to remote regions are still largely unknown. In particular, the influence of atmospheric aerosols (i.e., particles) on PAH long-range transport (LRT) is highly uncertain. A number of schemes have been proposed to estimate gas-particle distribution of PAHs, with each predicting different PAH LRT potential. Additionally, there is debate within the atmospheric chemistry literature regarding aerosol formation and evolution over time, and how best to simulate these processes. Here, we conduct simulations of atmospheric PAH transport using the chemical transport model GEOS-Chem with different assumptions about (1) gas-particle partitioning and (2) physicochemical characteristics of different aerosol types to test how these variables affect PAH LRT efficiency.

PAHs have been extensively measured in both gas and particle phases. Schemes for estimating measured phase distributions have evolved over time, as recently reviewed by Lohmann and Lammel[3] and Keyte et al.[4] To summarize, PAH gas-particle partitioning has been described with four different schemes, each assuming instantaneous equilibrium partitioning (EqP): (1) the Junge-Pankow adsorption scheme,[5-8] in which PAH adsorption to total suspended particles depends on the PAH sub-cooled liquid vapor pressure; (2) the Finizio scheme[9], which partitions PAHs to particles based on a gas-particle equilibrium partition coefficient (K_P=[PAH]$_{particle}$/[PAH]$_{gas}$) that is empirically related to the octanol-air partition coefficient (K_{OA}=[PAH]$_{octanol}$/[PAH]$_{air}$); (3) the Harner-Bidleman scheme,[10] which augments the Finizio scheme by accounting for the fraction of organic material (OM, used here interchangeably with "organic aerosol", or OA) within a particle; and finally, (4) the Dachs and Eisenreich ("D&E") scheme,[11] which considers both absorption into OM and adsorption to black/elemental carbon (BC) within the particle.

In general, the Junge-Pankow, Finizio, and Harner-Bidleman schemes underestimate particulate fractions and particle phase concentrations (i.e., they underpredict K_P), both when compared directly to observations[3, 12, 13] and when employed in atmospheric transport models.[14, 15] Schemes considering absorption into OM generally perform better than the

67 Junge-Pankow, however. The D&E scheme better represents observed PAH concentrations
68 and phase distributions in various comparisons,[3, 12, 14-16] especially in remote regions. This is
69 consistent with knowledge about PAH partitioning in the marine environment, where sorption
70 to sedimentary BC limits aquatic PAH concentrations, and thus, availability and toxicity to
71 marine organisms.[17-20] However, the D&E scheme cannot explain the observed lack of
72 correlation between particle and gas phases,[21] and can overpredict observed K_P values.[11]
73 Collectively, the inability of these partitioning schemes to accurately estimate PAH phase
74 distribution suggests the assumption of instantaneous equilibrium is inaccurate.

75   It has recently been suggested, based on laboratory studies, that PAHs become trapped
76 in secondary organic aerosol (SOA) during SOA formation, preventing them from
77 evaporating to the gas phase and protecting them from degradation via oxidation.[22] This
78 process could explain the observed lack of gas-particle correlation and generally low
79 estimated K_P values compared to measurements. Unlike primary organic aerosol (POA),
80 which is directly emitted to the atmosphere, SOA forms within the atmosphere. Thus, total
81 atmospheric organic aerosol (OA or OM) contains both POA and SOA. SOA has traditionally
82 been considered aerosol formed from the oxidation and condensation of gas-phase precursors,
83 including SVOCs such as PAHs. Recently, however, oxidation of gas-phase compounds that
84 have evaporated from POA has been recognized as another source of SOA.[23] SOA is
85 estimated to comprise over 30% of total atmospheric OM,[24] though this fraction may be much
86 greater if current estimates are missing key sources. The contribution of PAHs to SOA
87 formation could be significant in anthropogenically influenced locations. One study estimated
88 that PAHs account for >10% of SOA in Houston, TX (USA),[25] and another showed that
89 alkanes and PAHs combined may account for 20-30% of ground-level anthropogenic SOA in
90 the U.S.[26]

91   While PAH modeling studies use various schemes for representing gas-particle
92 partitioning, none explicitly consider the role of SOA on PAH LRT. Evaluating the impact of
93 SOA on PAHs is important from two different perspectives. First, if PAHs are trapped in
94 SOA during SOA formation, they may be shielded from oxidative degradation and prevented
95 from exchanging with the gas phase. This could explain why PAH K_P values are generally
96 underpredicted by EqP schemes. Second, OA models, including the GEOS-Chem model used
97 in the present study, tend to underestimate observed OA concentrations, implying potential

98   missing SOA sources.[24] Incorporation of PAHs during SOA formation has been found to

99   significantly decrease SOA evaporation rates,[22] potentially increasing SOA atmospheric

100 lifetimes and simulated OA concentrations, though we do not evaluate this.

101   Here, we use a global model to test the importance of SOA to PAH LRT, with the

102 hypothesis that incorporating SOA into the model will better reproduce observed gas-particle

103 distributions compared to a model that uses primary carbonaceous aerosols for partitioning.

104 We modify the previously developed and evaluated GEOS-Chem PAH model[27] to include

105 SOA partitioning, and compare results from the SOA-inclusive simulation to those from the

106 default simulation, which employs the D&E OM/BC absorption/adsorption EqP scheme. We

107 conduct additional sensitivity simulations to determine the importance of different PAH-

108 aerosol assumptions besides partitioning: aerosol deposition efficiencies; concentrations of

109 primary aerosols (OM/BC) versus SOA; and constant versus spatiotemporally varying oxidant

110 concentrations. We conduct all simulations for pyrene, given its semivolatility (i.e.,

111 substantial mass is found in both the gas and particle phases) and because its physicochemical

112 relationship with SOA has been evaluated extensively compared to other PAHs.[22]

113

114 ## Methods

115 **GEOS-Chem PAH model: default configuration**

116   The development and evaluation of the GEOS-Chem PAH model (v8-03-02) has been

117 described in full elsewhere.[27] To summarize, the model includes: oxidation of gas phase

118 PAHs by hydroxyl radical (OH; scaled for diurnal variation); oxidation of particle-phase

119 PAHs by ozone (O_3); wet and dry deposition of both gas and particle phase PAHs; and

120 temperature-dependent partitioning between the gas phase and two particle phases

121 (hydrophobic primary OM and BC) following the D&E scheme.[11] The particle phases used in

122 the default model are primary hydrophobic carbonaceous aerosols only; i.e., "primary OM"

123 refers to OM that does not include SOA. K_{OA}s are used to describe absorptive partitioning

124 between the gas and primary OM phases, and BC-air equilibrium partition coefficients

125 (K_{BC}=[PAH]$_{BC}$/[PAH]$_{gas}$) describe adsorptive partitioning between gas and BC. A separate

126 NO_x-Ox-hydrocarbon-aerosol version of GEOS-Chem (v9-01-02) is used to generate monthly

127 mean concentrations of OH, O_3, hydrophobic organic carbon (OC), and hydrophobic BC,

128 which are archived and read into the PAH model as input. Sensitivity simulations with daily

129 versus monthly oxidant and aerosol inputs suggest monthly averaging results in, at most, a 2%

130 change in PAH concentrations.[28] OC concentrations are multiplied by 1.8 to represent primary

131 OM[29]. OM and BC particles with which PAHs are associated convert from hydrophobic to

132 hydrophilic species with a lifetime of 1.2 days,[30] increasing the efficiency of wet scavenging

133 over time with no change in PAH chemistry. PAHs partition between the gas phase and

134 hydrophobic aerosols only; once particles become hydrophilic, PAHs remain associated with

135 the particle until depositing. In the default model, BC plays a much larger role than primary

136 OM in sequestering PAHs within the particle phase: 98% of particulate PAHs are associated

137 with BC rather than OM. A land-atmosphere exchange module was developed and employed

138 recently to evaluate the effect of climate on PAH transport;[28] to reduce variables in the

139 present study, however, we neglect land-atmosphere exchange, which results in minor (~1%)

140 decreases to simulated concentrations with no effect on partitioning. We use a global PAH

141 primary emissions inventory from 2004 compiled on a country-by-country basis, spatially

142 allocated on a 1°x1° grid,[31] and assimilated meteorology from the NASA Goddard Earth

143 Observing System's GEOS5 dataset degraded to 6 hours temporally, 4°x5° horizontally, and

144 47 levels vertically. All physicochemical constants used are shown in Table S1. We refer to

145 our standard PAH model using the D&E partitioning scheme as the "default" configuration.

146

Default configuration updates and modifications

148   The version of the model used here includes several updates relative to previously

149 published work.[27, 28] We include particle-phase oxidation by NO_3 (in addition to O_3) following

150 recently-published data.[32] We use monthly mean NO_3 concentrations archived from NO_x-O_x-

151 hydrocarbon-aerosol GEOS-Chem simulations, scaled for diurnal variation, and reaction rates

152 provided by Liu et al.[32] (Table S1). We also use improved Leaf Area Indices (LAI) for

153 calculating dry deposition fluxes. We evaluate the influence of including these processes on

154 simulated PAH concentrations relative to previous model versions in the SI (Figures S1 and

155 S2); in general, these updates improve model-measurement comparisons.

156

SOA-PAH configuration

158   We develop a separate configuration of the GEOS-Chem PAH model to address SOA

159 partitioning (the "SOA-PAH" configuration). We first generate global SOA concentrations

160 with the GEOS-Chem NO_x-O_x-hydrocarbon-aerosol model (v9-01-02).[33] GEOS-Chem

161 assumes sources of 23.4 Tg yr^{-1} biogenic and 3.1 Tg yr^{-1} anthropogenic SOA, which

162 combined is on the low end of SOA estimates.[24] This does not include a ~100 Tg yr^{-1} source

163 of "anthropogenically-enhanced" SOA that has been recommended for inclusion in models

164 based on reduced mean error between simulated SOA concentrations and measurements,[34, 35]

165 and we discuss uncertainties associated with this below. We archive monthly mean

166 concentrations of total SOA (mean of 2006-2008) for input to the PAH model. Simulated

167 SOA surface concentrations are generally several times greater than primary hydrophobic OM

168 and BC (Figure S3). For the SOA-PAH configuration, we simulate PAHs in two phases: a gas

169 phase, and a particle phase consisting solely of SOA-bound PAH (ignoring partitioning to

170 primary OM and BC). Gas-phase PAHs oxidize and deposit as described above and in our

171 previous PAH model studies.[27, 28] SOA-bound PAH is scavenged in convective updrafts,

172 rainout, and washout with an efficiency of 80% following Chung and Seinfeld,[36] consistent

173 with SOA behavior in GEOS-Chem.[24, 33] This differs from primary OM- and BC-bound PAHs

174 in the default simulation, which are wet scavenged at 0% efficiency while hydrophobic and

175 100% efficiency after becoming hydrophilic. Dry deposition is treated similar to the default

176 simulation, following a resistance-in-series scheme[37] with no size dependence.

177

178 **Simulations to evaluate partitioning**

179   We use the default and SOA-PAH configurations described above to run individual

180 simulations comparing the effect of these different partitioning schemes on PAH LRT. Table

181 1 lists these simulations under #1, with additional sensitivity simulations (discussed below)

182 under #2. Simulations employing the SOA-PAH configuration are divided into two emissions

183 scenarios based on uncertainties in phase distribution upon emission. In the default

184 configuration, PAHs are emitted as total mass (gas plus particle) and distributed

185 instantaneously between the gas and primary OM/BC phases according to K_{OA}, K_{BC}, and

186 ambient OM/BC concentrations within the boundary layer. This is a known source of

187 uncertainty, as in-situ measurements of the phase upon emission are limited or vary

188 substantially for most major PAH sources. Similarly, few data exist to suggest a suitable

189   approach for distributing emissions between gas and SOA phases. Thus, we construct two

190   emissions scenarios within the SOA-PAH configuration to capture a range of potential phase

191   distributions upon emission: (a) 100% of PAHs are trapped in SOA upon emission (denoted

192   "100% in SOA"), and (b) the fraction of PAH emissions trapped is determined by partitioning

193   between SOA and gas phases according to K_{OA} and boundary layer SOA concentrations

194   ("SOA/gas"). Both scenarios assume PAHs can only become trapped in SOA within the 4º x 5º

195   grid box into which PAHs are emitted. Though both scenarios may neglect entrapment after

196   LRT, the lifetimes of SOA precursors are short enough that SOA formation relevant to PAH

197   entrapment likely happens before substantial LRT has taken place; i.e., we assume the effect

198   is small.

199   After initial partitioning as described above, simulations employing the SOA-PAH

200   configuration use a chemistry and partitioning scheme following the experimental results of

201   Zelenyuk et al.[22] In contrast to the instantaneous EqP scheme of the default configuration,

202   PAHs in SOA-PAH simulations slowly evaporate from SOA after their initial entrapment.

203   According to Zelenyuk et al., ~50-80% of PAH trapped in SOA during SOA formation

204   remains associated with the particle after 24 hours, with 80% likely the more realistic estimate

205   given differences between laboratory and atmospheric conditions. We model this evaporation

206   process using an exponential decay function:

$$m(t) = m(0) \times e^{-kt}$$

207   (1)

208   where m(t) is the mass of SOA-bound PAH at time t, m(0) is the initial mass of SOA-bound

209   PAH, and k is the evaporation rate, which is set to correspond to 80% PAH remaining after 24

210   hours (unless otherwise noted). Zelenyuk et al. also estimated that only 10% of PAH

211   associated with SOA is on or near the particle surface. We thus assume for SOA-PAH

212   simulations that only 10% of SOA-associated PAHs are susceptible to heterogeneous particle-

213   phase oxidation, in contrast to the default configuration where 100% of primary OM and BC-

214   associated PAHs undergo oxidation. For both the default and SOA-PAH configurations, we

215   conduct simulations with and without particle-phase oxidation, and SOA-PAH simulations

216   are conducted under both emission scenarios (simulations 1a-1f under #1 in Table 1).

217   We note that there are several uncertainties associated with the Zelenyuk scheme that

218   have implications for results from SOA-PAH simulations, including the degree to which SOA

219 exists as a viscous, semi-solid substance in the atmosphere, which namely depends on

220 temperature and relative humidity[38] (Zelenyuk et al. conducted their experiments under dry

221 conditions). These uncertainties could modify the degree of PAH trapping and oxidation, and

222 lead to variations in resulting gas-particle ratios. We address this by running simulations with

223 an evaporation rate corresponding to 50% PAH remaining trapped after 24 hours, the lower

224 limit of the range mentioned above.

225

226 **Simulations to evaluate sensitivity to other model parameters**

227 We conduct three additional sensitivity simulations with the SOA-PAH configuration

228 to test the influence of parameters not directly related to partitioning scheme (simulations 2a-

229 2c, Table 1). These are: differences in wet deposition efficiency between primary OM/BC and

230 SOA; the influence of OH concentration; and the concentration/spatiotemporal difference

231 between OM/BC and SOA. To test the effect of differences in wet deposition efficiency,

232 which could affect particulate PAH lifetimes relevant to LRT, we replace the deposition

233 efficiency of SOA with that of hydrophobic OM/BC (simulation 2a, Table 1). OH

234 concentrations influence gas-phase degradation lifetimes. Some previous PAH modeling

235 exercises have assumed constant OH concentrations,[22] while others have found that seasonal

236 variations in OH can cause marked differences in PAH concentrations.[39] To diagnose the

237 influence of these assumptions we replace spatially- and temporally-varying OH

238 concentrations with a blanket OH concentration of 10^6 molecules/cm^3 (simulation 2b). Spatial

239 and temporal variability in aerosols could also affect transport pathways by changing particle

240 availability for partitioning, and thus, PAH gas-particle distribution. To assess differences in

241 the spatial and temporal distribution of hydrophobic primary aerosols versus SOA, we use

242 monthly mean archived concentrations of primary OM/BC in place of SOA concentrations

243 (simulation 2c).

244 The "100% in SOA" emission scenario is more sensitive than the "SOA/gas" scenario

245 to the effect of wet deposition, since it allocates a greater fraction of PAH (100%) to the

246 particulate phase, while the SOA/gas emission scenario has greater sensitivity to spatial and

247 temporal distribution of aerosol. The latter is because when PAHs are divided between gas

248 and particulate phases by K_{OA}, the fraction of particulate PAH is calculated according to the

249 volume ratio between air and particles; hence, particle concentrations need to be known. This

250 is in contrast to the 100% in SOA emissions scenario, where there is no dependence on

251 particle concentration because the PAH particulate fraction is assumed to be independent of

252 air-particle volume ratios. Finally, the SOA/gas emission scenario is more sensitive to

253 changes in OH, because a greater fraction of PAH exists in the gas phase. We thus use the

254 100% in SOA scenario for our wet deposition sensitivity simulations, and the SOA-gas

255 partitioning emission scenario for spatial and temporal distribution and OH sensitivity

256 simulations. Partitioning in the latter two sensitivity scenarios follows the SOA/gas emissions

257 scenario, using the K_{OA} alone to partition PAHs upon emission, even when primary OM/BC is

258 substituted for SOA (i.e., the K_{BC} is not used, so we can isolate the effect of aerosol

259 concentration/deposition versus difference in partitioning strength).

260

261 **Simulations to assess the role of instantaneous equilibrium partitioning versus aerosol**

262 **type: OM/BC-evap configuration**

263   In a final set of simulations (Table 1, #3), we evaluate the possibility that PAHs are

264 trapped in primary carbonaceous species (OM/BC) rather than SOA, with subsequent slow

265 evaporation following Eq. 1 as in the SOA-PAH configuration. In this configuration, termed

266 "OM/BC-evap", PAHs partition to ambient primary OM/BC when emitted following both the

267 K_{OA} and K_{BC}, and 80% of PAH remains in the particle after 24 hours. The OM/BC-evap

268 configuration isolates the effect of SOA versus BC (i.e., aerosol type) from the effect of EqP

269 because (1) the trapping scenario is used instead of EqP, and (2) in all simulations where

270 primary OM and BC represent the particle phase, BC-bound PAH accounts for 98% of the

271 particle phase budget; primary OM plays only a minor role in sequestering pyrene. We

272 conduct simulations with this "OM/BC-evap" configuration with and without particle-phase

273 oxidation (simulations 3a and 3b Table 1).

274 **Model evaluation**

275   To evaluate how well each simulation captures observed concentrations, we conduct

276 paired t-tests for differences between simulated and observed three-year (2006-2008) mean

277 total (gas+particulate) concentrations at northern hemisphere stations reporting at least

278 monthly measurements (see Table S2 for station information). We compare annual means

279 only at stations distant from sources (i.e., non-urban mid-latitude and Arctic sites). We also

280 compare simulated and observed monthly mean total concentrations from sites in Table S2 to

281 assess how well simulations capture seasonal variability at non-urban mid-latitude and Arctic

282 sites. Finally, we compare simulated and observed monthly mean particulate fractions (i.e.,

283 $[PAH]_{particulate}/[PAH]_{total}$). We make this comparison only at stations operated by the

284 Integrated Atmospheric Deposition Network (over the U.S. and Canadian Great Lakes), where

285 phase-resolved measurements are prioritized and considered reliable for model evaluation.

286

Results

288 **Statistical comparison of annual means**

289   Scatter plots of simulated versus observed mean concentrations are shown in Fig. S4,

290 while linear best-fit equations, correlation coefficients (r=0.65-0.70), and log mean biases

291 (LMB=-0.08-0.21) are shown in Table S3. Our default configuration is able to capture annual

292 mean PAH concentrations: for default simulations (1a and 1b, Table 1), there is no significant

293 difference (α=0.05) between simulated and observed annual means, both with and without

294 particle-phase oxidation turned on (p=0.97 and 0.07, respectively). Annual means from SOA-

295 PAH simulations using the SOA/gas emissions scenario (1e and 1f) also are not statistically

296 different from observed means (p=0.27 and 0.26 for with and without particle-phase

297 oxidation, respectively). In contrast, comparison of simulated and observed annual means

298 shows that simulating 100% PAH entrapment in SOA upon emission does not match

299 observations of LRT (1c and 1d). Annual means are significantly higher than observations for

300 SOA-PAH simulations when 100% of emissions are allocated to SOA: simulated

301 concentrations are 4.4x higher than observed with particle-phase oxidation (p=0.01) and 7.4x

302 higher without (p<0.01). These results confirm that if PAHs are indeed trapped in SOA upon

303 emission, it is unlikely that 100% of PAH becomes associated with SOA.

12

304   SOA-PAH simulations using an evaporation rate corresponding to 50% of particulate

305   PAH remaining after 24 hours (rather than the default of 80%) resulted in, at most, a 15%

306   decrease in simulated annual mean concentrations (data not shown). Though this is a

307   relatively minor change, we note that the 50-80% evaporation rate range used here was

308   obtained under dry conditions, which are unlikely in the atmosphere. Thus, true atmospheric

309   evaporation rates probably have even greater variability and could have stronger influence on

310   PAH concentrations.

311

312   **Monthly mean concentrations**

313   We compare monthly mean observed and simulated total concentrations and

314   particulate fractions to further assess simulations using different partitioning schemes (under

315   #1 in Table 1). Fig. 1A and 1B show simulated vs. observed monthly means at nonurban mid-

316   latitude and Arctic stations, respectively, while Fig. 1C compares simulated and observed

317   particulate fractions at IADN sites in the U.S./Canadian Great Lakes. Results from

318   simulations to evaluate partitioning (Table 1, 1a-1f; green, blue, and red lines in Fig. 1) are

319   compared to observations (black lines) in this section; simulations to evaluate the effect of

320   PAH trapping by BC (Table 1, 3a and 3b; purple lines in Fig. 1) are discussed later.

321   Comparison of simulated and observed monthly mid-latitude concentrations (Fig. 1A)

322   shows that phase distribution upon emission has more influence on PAH LRT than

323   partitioning behavior during transport. All simulations capture the inter-monthly trend in mid-

324   latitude concentrations (more in winter, less in summer). Simulations in which PAHs are

325   partitioned between gas and particle phases upon emission (1a, 1b, 1e, and 1f, Table 1; green

326   and red lines, Fig. 1A) result in concentrations that fall within +/- one standard deviation of

327   monthly means, regardless of whether they are partitioned to primary OM/BC or SOA, and

328   whether they following the default EqP scheme or the SOA-PAH scheme. Consistent with the

329   annual mean comparison, SOA-PAH simulations following the 100% in SOA emissions

330   scenario (1c and 1d, Table 1; blue lines, Fig. 1A) overestimate measured values. Including

331   particle-phase oxidation (dotted lines) does not substantially change results.

332   In contrast to mid-latitude concentrations, comparisons to monthly mean Arctic

333   concentrations (Fig. 1B) show that when larger fractions of PAH are distributed to the particle

334 phase upon emission and protected from oxidation there is a better match to observations. All

335 simulations generally capture concentrations during colder months within +/- one standard

336 deviation of measured means, but underestimate summer concentrations by up to ~100x.

337 Summer underestimates are likely partially due to the influence of local sources not included

338 in model emissions (e.g., camp or wildfires).[40] Simulated concentrations are generally higher,

339 and closer to Arctic measured values, when a greater fraction of PAH is allocated to the

340 particle phase when emitted and protected from oxidation. Thus, in contrast to annual mean

341 and mid-latitude monthly comparisons, the SOA-PAH 100% in SOA scenario performs best,

342 consistent with the hypothesis that trapping of PAHs in SOA may account for high particulate

343 fractions in remote areas.[22] Similar to the mid-latitudes, however, simulated transport to the

344 Arctic is more strongly influenced by distribution upon emission than partitioning scheme

345 subsequent to emission; e.g., simulations 1a and 1e, the green and red solid lines in Fig. 1,

346 which partition PAH upon emission to primary OM/BC and SOA, respectively, show nearly

347 identical results, despite different partitioning behavior during transport.

348   Comparison with particulate fractions shows that the SOA-PAH configurations under-

349 and overestimate particulate fraction while the default configuration performs best (Fig. 1C).

350 Default simulations (1a and 1b, Table 1) predict particulate fractions closest to measured

351 values and capture the inter-monthly trend of higher particulate fractions in winter versus

352 summer most accurately (green lines, Fig. 1C). The particulate fraction is highly

353 overestimated by SOA-PAH simulations with 100% of emissions in SOA, even when

354 particle-phase oxidation is turned on (1c and 1d, Table 1, and solid and dotted blue lines, Fig.

355 1C, respectively). The SOA-PAH 100% entrapment scenario also fails to capture seasonal

356 variation in particulate fraction, predicting higher fractions in summer versus winter, whereas

357 observed particulate fraction is lowest in summer. In contrast, particulate fractions are

358 severely underestimated in the SOA/gas scenario (simulation 1e; red solid line, Fig. 1C),

359 especially when oxidation is implemented (simulation 1f; red dotted line, Fig. 1C; >10x lower

360 than mean measured values).

361   Although concentration and phase distribution results suggest allocating more PAH to

362 the particulate phase during emission increases LRT, they also imply the two have a complex

363 relationship. This can be observed by comparing 100% in SOA simulations with and without

364 particle phase oxidation (1c and 1d, Table 1). Implementing particle phase oxidation does not

365 affect the extreme overestimates of particulate fraction (blue lines, Fig. 1C), but causes

366 notable decreases in concentrations (blue lines, Fig. 1A and 1B). That is, nearly identical

367 particle phase fractions exhibit different LRT results. Another example is seen when default

368 simulations are compared to SOA/gas emissions scenario simulations (1a and 1b to 1e and 1f,

369 respectively). Simulated particulate fractions vary dramatically between these two

370 configurations (green and red lines, Fig. 1C), but predicted total concentrations are very

371 similar (green and red lines, Fig. 1A and 1B). Thus, different particle phase fractions result in

372 similar total LRT. This complex relationship between phase distribution and total PAH

373 transport has been noted in other PAH modeling studies comparing different partitioning

374 parameterizations.[16] Thus, our results suggest the amount of PAH partitioning to particles

375 cannot alone be used to predict LRT potential.

376   Arctic particulate fractions from different simulations (Fig. S5) have distinctly

377 different seasonal patterns. We do not compare these to observations, however, as Arctic

378 sampling requires high airflow rates and long sampling periods, which can cause phase

379 resolution artifacts. Similar to mid-latitude results, 100% in SOA simulations (1d and 1e)

380 produce the highest particulate fractions (blue lines, Fig. S5), though overall particulate

381 fraction is smaller in the Arctic than at mid-latitudes. The particulate fraction for SOA-PAH

382 simulations (blue and red lines) are maximum in summer, while default simulations (green

383 lines) are minimum in summer. While data to constrain seasonal variations in Arctic

384 particulate fraction have methodological limitations, as noted above, Sofowote et al.[40] found

385 that pyrene Arctic particulate fraction was maximum in summer and minimum in winter,

386 opposite of that found in the mid-latitudes. Sofowote et al. attributed the summer-time

387 maximum to a shift to local emissions sources (not included in our model emissions).

388 However, this nevertheless suggests SOA-PAH simulations capture the seasonal trend in

389 Arctic particulate fraction better than default simulations.

390

391 **Effect of factors other than partitioning**

392   Sensitivity simulations suggest interaction with primary aerosols rather than SOA is

393 more important than the influence of wet deposition efficiency or spatiotemporal variation in

394 OH concentrations for matching observed phase distributions. Fig. 2 shows the results of this

395   sensitivity simulation (simulation 2c, Table 1) compared with observations. Also shown for

396   comparison are default and SOA/gas results for simulations without particle-phase oxidation

397   (i.e., simulations 1a and 1e from Table 1; solid green and red lines from Fig. 1). Results of the

398   other two sensitivity simulations are shown (Fig. S6) and discussed in the SI.

399   Substituting primary OM/BC concentrations for SOA (red line with circles) causes

400   very little change in total concentration (<1% increase in both the mid-latitudes and Arctic;

401   Fig. 2A and 2B), but there is an average increase (17%) in particulate fraction (Fig. 2C),

402   which better matches observations. More important, the seasonal pattern of particulate

403   fraction in the primary OM/BC concentration sensitivity simulation better matches

404   observations. This is consistent with seasonal trends for aerosols: SOA tends to be higher in

405   summer because emissions correlate with temperature, while primary carbonaceous aerosols

406   often peak in winter because of burning for heat. This suggests interaction with primary

407   aerosols rather than SOA is what drives the better match to observed phase distributions in the

408   default simulation. We note that the addition of greater sources of anthropogenically

409   controlled SOA to OA models has been recommended in the past,[35] and it is possible that

410   anthropogenically controlled SOA could exert similar controls on PAH LRT as primary

411   aerosols. We discuss the potential influence of including these sources[34, 35] below.

412

413   **Assessing the role of instantaneous equilibrium partitioning versus aerosol type**

414   The OM/BC-evap simulation with no particle-phase oxidation, (3a, Table 1; purple

415   lines, Fig. 1) agrees better than the default configuration (green lines, Fig. 1) with observed

416   phase distribution (Fig. 1C) and Arctic concentrations (Fig. 1B). Mid-latitude results (Fig. 1A)

417   are biased high, however, and there is a significant difference between annual simulated and

418   observed means (p=0.03; Fig. S4). Turning on particle-phase oxidation (simulation 3b)

419   improves mid-latitude seasonal (Fig. 1A) and annual concentrations, such that there is no

420   longer a significant difference between annual means (p=0.07; Fig. S4), but the match to

421   remote observations degrades, as does the match to phase distribution (Fig. 1B and 1C).

422   The OM/BC-evap configuration substantially increases Arctic particulate fractions

423   compared to the default configuration (e.g., from an annual mean of 0.02 for simulation 1a to

424   0.4 for simulation 3a), and reverses the seasonal pattern (Fig. S5). The OM/BC-evap

425 configuration produces an Arctic particle phase maximum in summer consistent with what

426 Sofowote et al.[40] observed for pyrene. Thus, the OM/BC-evap configuration captures mid-

427 latitude and remote concentrations and phase distributions simultaneously with the most skill.

428

Discussion

The role of black carbon

431   Our results demonstrate that trapping PAHs in carbonaceous aerosols upon emission

432 improves agreement between measured and simulated PAH concentrations in remote regions

433 and particle phase distributions, compared to a scheme that uses EqP. Simulations employing

434 SOA as the sole particle phase to which PAHs partition result in PAH particulate fractions

435 that are either too high or too low compared to observations, however, and with the opposite

436 seasonal pattern. In contrast, default simulations with EqP between the gas phase and primary

437 hydrophobic carbonaceous aerosols (OM/BC) closely capture particulate fraction magnitude

438 and seasonal variation as well as mid-latitude total concentrations, but underestimate remote

439 concentrations. Thus, we created a configuration ("OM/BC-evap") that explicitly considers

440 adsorption to BC (i.e., with the K_{BC}) to test whether the strong sorption to BC versus SOA

441 was the main reason for better particulate phase model-observation agreement with the default

442 configuration (versus EqP). Indeed, simulating entrapment of PAHs by BC and limiting

443 exchange with the gas phase provides the best match to all observations, especially with

444 respect to magnitude and seasonality of phase distribution. Exchange with the gas phase

445 during transport has only a small influence on ability to reproduce measurements.

446 Collectively, our results suggest two considerations of primary importance in determining

447 PAH LRT, with a particular emphasis on the role of BC: 1) physicochemical behavior

448 governing initial PAH association with particles (i.e., magnitude of partition coefficients and a

449 particle's ability to sequester/trap PAHs during emission), and 2) particle concentrations close

450 to or within emission sources.

451   Evidence of BC's importance to PAH LRT can be found in the similarity between

452 simulations distributing PAH between the gas and aerosol phases upon emission. Default (1a

453 and 1b) and SOA-gas emission scenarios (1e and 1f) predict remarkably similar concentration

454 results, both in the mid-latitudes and Arctic, compared with simulations trapping 100% of

455   PAH in SOA upon emission (1c and 1d). This suggests that PAH gas-particle distribution

456   upon emission is a key process determining how PAHs transport, and PAHs are much more

457   likely associated with BC versus SOA when emitted. Activities producing the greatest PAHs

458   emissions globally are also those producing large quantities of BC,[31, 41] namely combustion of

459   bio- and fossil fuels. Indeed, there is a large amount of literature demonstrating pyrogenic

460   PAHs and BC (or soot) are co-emitted, with strong evidence that PAHs are molecular

461   intermediates in the process of BC formation and growth during combustion.[42] While PAHs

462   also have petrogenic and biogenic sources, globally these are minor compared to pyrogenic.[31]

463   An important role for atmospheric BC is consistent with PAH behavior in

464   aquatic/sediment environments, and also with results of other studies of PAH partitioning in

465   the air beyond the D&E study. For example, Arp et al.[43] investigated over 500 measured K_P

466   values for a wide range of SVOCs, including PAHs. Their results indicated that for most

467   neutral SVOCs, the water-insoluble OM fraction of aerosol was a good predictor of K_P. PAHs,

468   however, exhibited anomalous behavior in that measured K_Ps were up to ~100x higher than

469   predicted, which was attributed to a non-exchangeable fraction associated with BC. Indeed,

470   PAHs were the only SVOCs studied that are co-emitted with BC.

471

Uncertainties

473   The interpretation of our results is subject to a number of uncertainties. First, we do

474   not account for particle size, relative humidity, or particle heterogeneity. PAHs associated

475   with different particle sizes can deposit differently,[44] while humidity can impact oxidation

476   rates[45, 46] and diffusion of PAHs to particle surfaces.[38] Within the GEOS-Chem PAH model,

477   primary carbonaceous aerosols consist solely of hydrophobic OM and BC, when in reality

478   aerosols are only partially comprised of these components and can contain a number of other

479   phases, such as minerals and salts.[42, 47] Furthermore, the mixing of OM and BC within a single

480   particle from aging could affect PAH partitioning substantially. For example, OM coatings

481   that develop during transport could either diminish PAH adsorption to BC during transport or

482   trap PAHs already associated with BC. Concentrations of primary carbonaceous aerosols,

483   SOA, and oxidants in the PAH model are subject to the uncertainties of the GEOS-Chem

484   NO_x-Ox-hydrocarbon-aerosol model[24, 30, 48] with which they were generated.

485   We extend observations of SOA trapping of pyrene, determined via experiments with

486   SOA generated from α-pinene,[22] to BC in our final OM/BC-evap simulations. Given

487   differences between the formation of SOA and BC, it is likely that pyrene-BC interactions

488   differ considerably from pyrene-α-pinene interactions. The process of SOA formation itself is

489   largely unknown, with ongoing debate as to whether SOA is a semi-solid or liquid and

490   whether it is formed primarily from the oxidation of gas-phase precursors or from previously

491   emitted particles. The degree to which PAHs take part in SOA formation is still largely

492   unknown as well, and extending observations of PAH entrapment in SOA to BC adds yet

493   another layer of uncertainty. We acknowledge that our OM/BC-evap configuration may

494   represent a process for which there is little physical evidence in the atmosphere, but

495   nonetheless the simulations provide valuable information regarding agreement between

496   observations in mid-latitude and remote regions.

497   Additionally, it is possible that introducing greater sources of "anthropogenically

498   enhanced" SOA into the model could produce a PAH phase distribution similar to what we

499   observe with BC. Spracklen et al.[35] recommended adding a ~100 Tg/yr of anthropogenically-

500   controlled SOA to model sources to minimize SOA observation-model discrepancies. Heald

501   et al.[24] did just that with the GEOS-Chem SOA model, using simulated aromatic SOA as a

502   proxy for anthropogenically controlled SOA, and found dramatically better measurement-

503   model agreement near sources, but overestimates aloft and in remote regions. We note that

504   anthropogenically derived SOA and BC sources are likely correlated, and thus, the improved

505   phase distribution model-measurement agreement seen when PAHs partition primarily to BC

506   might also be observed if simulations were conducted with additional anthropogenically

507   controlled SOA instead.

508   There are uncertainties in pyrene oxidation rates in both the gas and particle phases

509   beyond the impact of humidity. For example, the gas phase OH reaction rate constant we use

510   for pyrene has been deduced from ionization potential[49] rather than empirically determined,

511   and particle phase oxidation rate constants have been measured for PAHs associated with

512   model substrates such as decanol, graphite, or diesel, rather than ambient particulate matter.[32,]

513   [50-52] These uncertainties could cause considerable variation in the loss of both the gas and

514   particle phases.

515   Finally, there are uncertainties in emissions, both in magnitude and spatial/temporal

516   distribution, which could lead to deviations in simulation performance. Sensitivity simulations

517   conducted with +/-20% of baseline emissions, however, demonstrate no notable change in

518   phase distribution. This suggests gas-particle distributions depend more strongly on PAH and

519   particle physicochemical behavior and phase distribution when emitted than emissions

520   magnitude.

521

Supporting Information Available

523   The supporting information includes physicochemical constants, measurement station

524   data, model and measurement correlation data, and comparison of previous model version

525   results to those presented here. This information is available free of charge via the Internet at

526   http://pubs.acs.org/.

527

Acknowledgments

532

References

533   1.   Halsall, C. J.; Barrie, L. A.; Fellin, P.; Muir, D. G. C.; Billeck, B. N.; Lockhart, L.;
Rovinsky, F.; Kononov, E.; Pastukhov, B. Spatial and temporal variation of polycyclic
aromatic hydrocarbons in the Arctic atmosphere. *Environ. Sci. Technol.* **1997,** *31*, 3593-3599.

2.   Wang, R.; Tao, S.; Wang, B.; Yang, Y.; Lang, C.; Zhang, Y.; Hu, J.; Ma, J.; Hung, H.
Sources and pathways of polycyclic aromatic hydrocarbons transported to Alert, the Candian
High Arctic. *Environ. Sci. Technol.* **2010,** *44*, 1017-1022.

3.   Lohmann, R.; Lammel, G. Adsorptive and absorptive contributions to the gas-particle
partitioning of polycyclic aromatic hydrocarbons: State of knowledge and recommended
parametrization for modeling. *Environ. Sci. Technol.* **2004,** *38*, 3793-3803.

4.   Keyte, I. J.; Harrison, R. M.; Lammel, G. Chemical reactivity and long-range transport
potential of polycyclic aromatic hydrocarbons - a review. *Chem. Soc. Rev.* **2013**.

5.   Junge, C. E., *Fate of Pollutants in the Air and Water Environment*. Wiley: New York,
1977; Vol. Part 1, pp 7-25.

6.   Pankow, J. F. Review and comparative-analysis of the theories on partitioning between
the gas and aerosol particulate phases in the atmosphere. *Atmos. Environ.* **1987,** *21*, 2275-
2283.

7.   Pankow, J. F. An absorption-model of gas-particle partitioning of organic compounds
in the atmosphere. *Atmos. Environ.* **1994,** *28*, 185-188.

8.   Pankow, J. F. An absorption-model of the gas aerosol partitioning involved in the
formation of secondary organic aerosol. *Atmos. Environ.* **1994,** *28*, 189-193.

9.   Finizio, A.; Mackay, D.; Bidleman, T.; Harner, T. Octanol-air partition coefficient as a
predictor of partitioning of semi-volatile organic chemicals to aerosols. *Atmos. Environ.* **1997,**
31, (15), 2289-2296.

10.   Harner, T.; Bidleman, T. F. Octanol-air partition coefficient for describing particle/gas
partitioning of aromatic compounds in urban air. *Environ. Sci. Technol.* **1998,** *32*, 1494-1502.

11.   Dachs, J.; Eisenreich, S. J. Adsorption onto aerosol soot carbon dominates gas-particle
partitioning of polycyclic aromatic hydrocarbons. *Environ. Sci. Technol.* **2000,** *34*, 3690-
3697.

12.   Wang, W.; Massey Simonich, S. L.; Wang, W.; Giri, B.; Zhao, J.; Xue; Cao, J.; Lu,
X.; Tao, S. Atmospheric polycyclic aromatic hydrocarbon concentrations and gas/particle
partitioning at background, rural village and urban sites in the North China Plain. *Atmos. Res.*
2011, *99*, 197-206.

13.   Lammel, G.; Klánová, J.; Ilić, P.; Kohoutek, J.; Gašić, B.; Kovacić, I.; Skrdlíková, L.
Polycyclic aromatic hydrocarbons in air on small spatial and temporal scales - II. Mass size
distributions and gas-particle partitioning. *Atmos. Environ.* **2010,** *44*, 5022-5027.

14.   Lammel, G.; Sehili, A. M.; Bond, T. C.; Feichter, J.; Grassl, H. Gas/particle
partitioning and global distribution of polycyclic aromatic hydrocarbons- A modelling
approach. *Chemosphere* **2009,** *76*, 98-106.

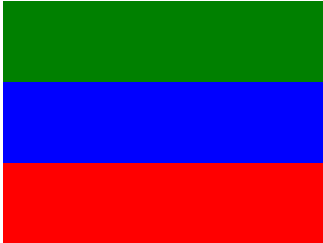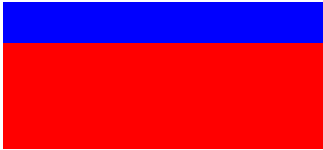15.   Sehili, A. M.; Lammel, G. Global fate and distribution of polycyclic aromatic

572 hydrocarbons emitted from Europe and Russia. *Atmos. Environ.* **2007,** *41*, 8301-8315.

573 16.   Galarneau, E.; Makar, P. A.; Zheng, Q.; Narayan, J.; Zhang, J.; Moran, M. D.; Bari,
574 M. A.; Pathela, S.; Chen, A.; Chlumsky, R. PAH concentrations simulated with the
575 AURAMS-PAH chemical transport model over Canada and the USA. *Atmos. Chem. Phys.*
576 *Discuss.* **2013,** *13*, 18417-18449.

577 17.   Jonker, M. T. O.; Koelmans, A. A. Sorption of polycyclic aromatic hydrocarbons and
578 polychlorinated biphenyls to soot and soot-like materials in the aqueous environment
579 mechanistic considerations. *Environ. Sci. Technol.* **2002,** *36*, 3725-3734.

580 18.   Gustafsson, O.; Haghseta, F.; Chan, C.; MacFarlane, J.; Gschwend, P. M.
581 Quantification of the dilute sedimentary soot phase: Implications for PAH speciation and
582 bioavailability. *Environ. Sci. Technol.* **1996,** *31*, (1), 203-209.

583 19.   Accardi-Dey, A.; Gschwend, P. M. Assessing the combined roles of natural organic
584 matter and black carbon as sorbents in sediments. *Environ. Sci. Technol.* **2002,** *36*, (1), 21-29.

585 20.   Cornelissen, G.; Gustafsson, O.; Bucheli, T. D.; Jonker, M. T. O.; Koelmans, A. A.;
586 Van Noort, P. C. M. Extensive sorption of organic compounds to black carbon, coal, and
587 kerogen in sediments and soils: Mechanisms and consequences for distribution,
588 bioaccumulation, and biodegradation. *Environ. Sci. Technol.* **2005,** *39*, (18), 6881-6895.

589 21.   Primbs, T.; Piekarz, A.; Wilson, G.; Schmedding, D.; Higginbotham, C.; Field, J.;
590 Simonich, S. M. Influence of Asian and Western United States urban areas and fires on the
591 atmospheric transport of polycyclic aromatic hydrocarbons, polychlorinated biphenyls, and
592 fluorotelomer alcohols in the Western United States. *Environ. Sci. Technol.* **2008,** *42*, 6385-
593 6391.

594 22.   Zelenyuk, A.; Imre, D.; Beranek, J.; Abramson, E. H.; Wilson, J.; Shrivastava, M.
595 Synergy between secondary organic aerosols and long-range transport of polycyclic aromatic
596 hydrocarbons. *Environ. Sci. Technol.* **2012,** *46*, 12459-12466.

597 23.   Robinson, A. L.; Donahue, N. M.; Shrivastava, M. K.; Weitkamp, E. A.; Sage, A. M.;
598 Grieshop, A. P.; Lane, T. E.; Pierce, J. R.; Pandis, S. N. Rethinking organic aerosols:
599 Semivolatile emissions and photochemical aging. *Science* **2007,** *315*, (5816), 1259-1262.

600 24.   Heald, C. L.; Coe, H.; Jimenez, J. L.; Weber, R. J.; Bahreini, R.; Middlebrook, A. M.;
601 Russell, L. M.; Jolleys, M.; Fu, T.-M.; Allan, J. D.; Bower, K. N.; Capes, G.; Crosier, J.;
602 Morgan, W. T.; Robinson, N. H.; Williams, P. I.; Cubison, M. J.; DeCarlo, P. F.; Dunlea, E. J.
603 Exploring the vertical profile of atmospheric organic aerosol: comparing 17 aircraft field
604 campaigns with a global model. *Atmos. Chem. Phys.* **2011,** *11*, 12673-12696.

605 25.   Shakya, K. M.; Griffin, R. J. Secondary organic aerosol from photooxidation of
606 polycyclic aromatic hydrocarbons. *Environ. Sci. Technol.* **2010,** *44*, 8134-8139.

607 26.   Pye, H. O. T.; Pouliot, G. A. Modeling the role of alkanes, polycyclic aromatic
608 hydrocarbons, and their oligomers in secondary organic aerosol formation. *Environ. Sci.*
609 *Technol.* **2012,** *46*, 6041-6047.

610 27.   Friedman, C. L.; Selin, N. E. Long-range atmospheric transport of polycyclic aromatic
611 hydrocarbons: A global 3-D model analysis including evaluation of Arctic sources. *Environ.*
612 *Sci. Technol.* **2012,** *46*, 9501-9510.

613 28.   Friedman, C. L.; Selin, N. E. Climate change and emissions impacts on atmospheric

614   PAH transport to the Arctic. *Environ. Sci. Technol.* **2014,** *48*, 429-437.

615   29.   Zhang, Q.; Worsnop, D. R.; Canagaratna, M. R.; Jimenez, J. L. Hydrocarbon-like and
616   oxygenated organic aerosols in Pittsburgh: insights into sources and processes of organic
617   aerosols. *Atmos. Chem. Phys.* **2005,** *5*, 3289-3311.

618   30.   Park, R. J.; Jacob, D. J.; Chin, M.; Martin, R. V. Sources of carbonaceous aerosols
619   over the United States and implications for natural visibility. *J. Geophys. Res.* **2003,**
620   *108(D12)*, 4355.

621   31.   Zhang, Y.; Tao, S. Global atmospheric emission inventory of polycyclic aromatic
622   hydrocarbons (PAHs) for 2004. *Atmos. Environ.* **2009,** *43*, 812-819.

623   32.   Liu, C.; Zhang, P.; Yang, B.; Wang, Y. X.; Shu, J. Kinetic studies of heterogeneous
624   reactions of polycyclic aromatic hydrocarbon aerosols with NO_3 radicals. *Environ. Sci.*
625   *Technol.* **2012,** *46*, 7575-7580.

626   33.   Wainwright, C. D.; Pierce, J. R.; Liggio, J.; Strawbridge, K. B.; Macdonald, A. M.;
627   Leaitch, R. W. The effect of model spatial resolution on Secondary Organic Aerosol
628   predictions: a case study at Whistler, BC, Canada. *Atmos. Chem. Phys.* **2012,** *12*, 10911-
629   10923.

630   34.   D'Andrea, S. D.; Hakkinen, S. A. K.; Westervelt, D. M.; Kuang, C.; Levin, E. J. T.;
631   Leaitch, W. R.; Spracklen, D. V.; Riipinen, I.; Pierce, J. R. Understanding and constraining
632   global secondary organic aerosol amount and size-resolved condensational behavior. *Atmos.*
633   *Chem. Phys. Discuss.* **2013,** *13*, 18969-19007.

634   35.   Spracklen, D. V.; Jimenez, J. L.; Carslaw, K. S.; Worsnop, D. R.; Evans, M. J.; Mann,
635   G. W.; Zhang, Q.; Canagaratna, M. R.; Allan, J.; Coe, H.; McFiggans, G.; Rap, A.; Forster, P.
636   Aerosol mass spectrometer constraint on the global secondary organic aerosol budget. *Atmos.*
637   *Chem. Phys.* **2011,** *11*, 12109-12136.

638   36.   Chung, S. H.; Seinfeld, J. H. Global distribution and climate forcing of carbonaceous
639   aerosols. *J. Geophys. Res.-Atmos.* **2002,** *107*, 4407.

640   37.   Wesely, M. L. Parameterization of surface resistances to gaseous dry deposition in
641   regional-scale numerical models. *Atmos. Environ.* **1989,** *23*, 1293-1304.

642   38.   Shiraiwa, M.; Ammann, M.; Koop, T.; Pöschl, U. Gas uptake and chemical aging of
643   semisolid organic aerosol particles. *PNAS* **2011**.

644   39.   Halsall, C. J.; Sweetman, A. J.; Barrie, L. A.; Jones, K. C. Modelling the behaviour of
645   PAHs during atmospheric transport from the UK to the Arctic. *Atmos. Environ.* **2001,** *35*,
646   255-267.

647   40.   Sofowote, U. M.; Hung, H.; Rastogi, A. K.; Westgate, J. N.; Su, Y.; Sverko, E.; D'Sa,
648   I.; Roach, P.; Fellin, P.; McCarry, B. E. The gas/particle partitioning of polycyclic aromatic
649   hydrocarbons collected at a sub-Arctic site in Canada. *Atmos. Environ.* **2010,** *44*, 4919-4926.

650   41.   Bond, T. C.; Bhardwaj, E.; Dong, R.; Jogani, R.; Jung, S.; Roden, C.; Streets, D. G.;
651   Trautmann, N. M. Historical emissions of black and organic carbon aerosol from energy-
652   related combustion, 1850-2000. *Global Biogeochem. Cycles* **2007,** *21*, GB2018.

653   42.   Seinfeld, J. H.; Pandis, S. N., *Atmospheric Chemistry and Physics*. 2nd ed.; John
654   Wiley & Sons, Inc.: Hoboken, New Jersey, 2006.

655 43. Arp, H. P. H.; Schwarzenbach, R. P.; Goss, K.-U. Ambient gas/particle partitioning. 2:
656 The influence of particle source and temperature on sorption to dry terrestrial aerosols.
657 *Environ. Sci. Technol.* **2008,** *42*, 5951-5957.

658 44. Kaupp, H.; McLachlan, M. S. Atmospheric particle size distributions of
659 polychlorinated dibenzo-p-dioxins and dibenzofurans (PCDD/Fs) and polycyclic aromatic
660 hydrocarbons (PAHs) and their implications for wet and dry deposition. *Atmos. Environ.*
661 **1998,** *33*, 85-95.

662 45. Shiraiwa, M.; Garland, R. M.; Pöschl, U. Kinetic double-layer model of aerosol
663 surface chemistry and gas-particle interactions (K2-SURF): Degradation of polycyclic
664 aromatic hydrocarbons exposed to O_3, NO_2, H_2O, OH and NO_3. *Atmos. Chem. Phys.* **2009,** *9*,
665 9571-9586.

666 46. Pöschl, U.; Letzel, T.; Schauer, C.; Niessner, R. Interaction of ozone and water vapor
667 with spark discharge soot aerosol particles coated with benzo[a]pyrene: O_3 and H_2O
668 adsportion, benzo[a]pyrene degradation, and atmospheric implications. *J. Phys. Chem. A*
669 **2001,** *105*, 4029-4041.

670 47. Gotz, C. W.; Scheringer, M.; MacLeod, M.; Roth, C. M.; Hungerbuhler, K. Alternative
671 Approaches for Modeling Gas-Particle Partitioning of Semivolatile Organic Chemicals:
672 Model Development and Comparison. *Environ. Sci. Technol.* **2007,** *41*, 1272-1278.

673 48. Bey, I.; Jacob, D. J.; Yantosca, R. M.; Logan, J. A.; Field, B.; Fiore, A. M.; Li, Q.;
674 Liu, H. X.; Mickley, L. J.; Schultz, M. Global modeling of tropospheric chemistry with
675 assimilated meteorology: Model description and evaluation. *J. Geophys. Res.* **2001,** *106*,
676 23,073-23,096.

677 49. EPA, U. S. Estimation Programs Interface Suite for Microsoft Windows, v 4.10.
678 United States Environmental Protection Agency, Washington DC, USA. **2011**.

679 50. Kahan, T. F.; Kwamena, N.-O. A.; Donaldson, D. J. Heterogeneous ozonation kinetics
680 of polycyclic aromatic hydrocarbons on organic films. *Atmos. Environ.* **2006,** *40*, 3448-3459.

681 51. Esteve, W.; Budzinski, H.; Villenave, E. Relative rate constants for the heterogeneous
682 reactions of OH, NO2 and NO radicals with polycyclic aromatic hydrocarbons adsorbed on
683 carbonaceous particles. Part 1: PAHs adsorbed on 1-2 mu m calibrated graphite particles.
684 *Atmos. Environ.* **2004,** *38*, 6063-6072.

685 52. Esteve, W.; Budzinski, H.; Villenave, E. Relative rate constants for the heterogeneous
686 reactions of NO2 and OH radicals with polycyclic aromatic hydrocarbons adsorbed on
687 carbonaceous particles. Part 2: PAHs adsorbed on diesel particulate exhaust SRM 1650a.
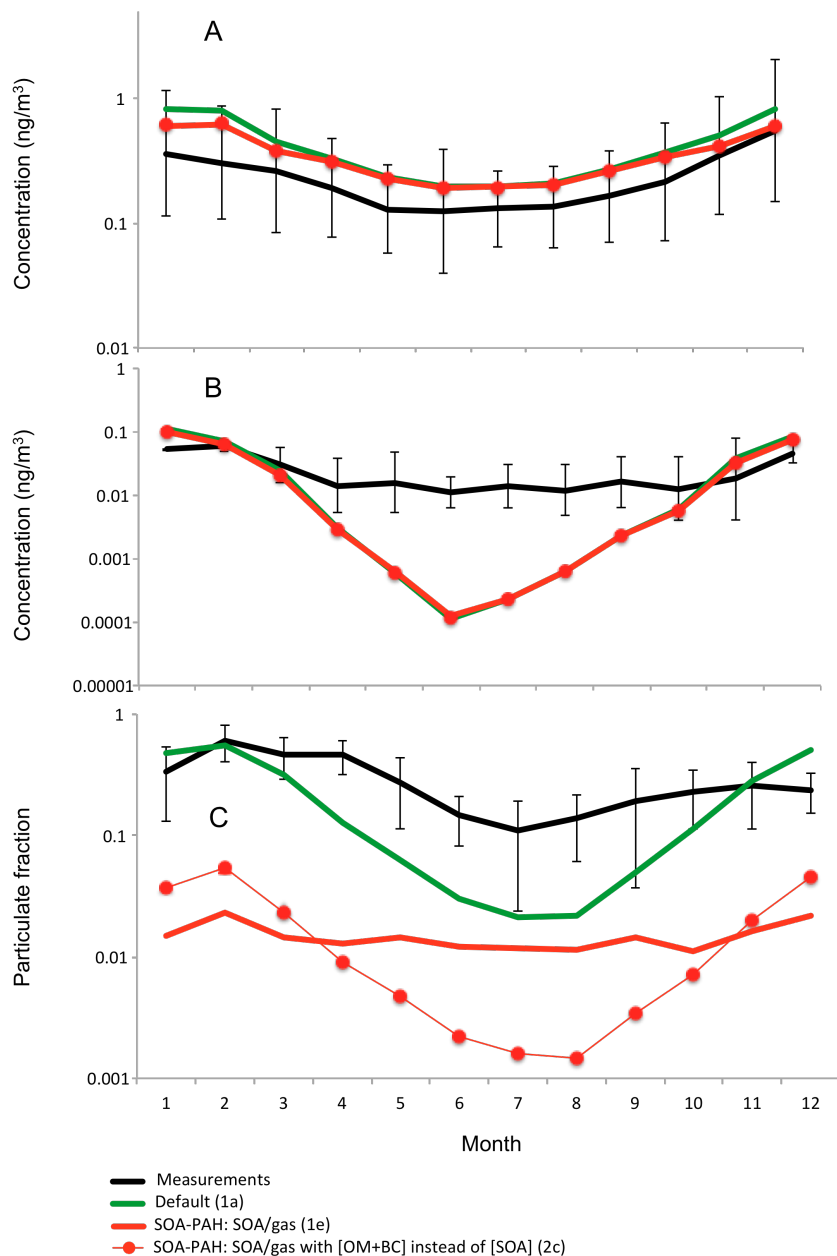688 *Atmos. Environ.* **2006,** *40*, 201-211.

689

690

690 **Tables**

691

Simulation	Model configuration	Emission scenario	Instantaneous EqP?	% of PAH available for particle-phase oxidation	Additional details	Color in figures
1. SIMULATIONS TO EVALUATE PARTITIONING						
1a	Default	OM, BC, and gas	Yes	0%		
1b	Default	OM, BC, and gas	Yes	100%		
1c	SOA-PAH	100% in SOA	No	0%		
1d	SOA-PAH	100% in SOA	No	10%		
1e	SOA-PAH	SOA/gas	No	0%		
1f	SOA-PAH	SOA/gas	No	10%		
2. SIMULATIONS TO EVALUATE SENSITIVITY TO OTHER MODEL PARAMETERS						
2a*	SOA-PAH	100% in SOA	No	0%	OM/BC wet deposition efficiency substituted for SOA	
2b*	SOA-PAH	SOA/gas	No	0%	Constant OH concentration	
2c	SOA-PAH	SOA/gas	No	0%	Sum of OM/BC concentrations in place of SOA concentrations	
3. SIMULATIONS TO EVALUATE THE ROLE OF INSTANTANEOUS EQUILIBRIUM PARTITIONING VERSUS AEROSOL TYPE						
3a	OM/BC-evap	OM, BC, and gas	No	0%	Default model without equilibrium partitioning	
3b	OM/BC-evap	OM, BC, and gas	No	10%	Default model without equilibrium partitioning	

692 **Table 1.** Summary of simulations conducted in this study. *Simulation results presented in the Supporting Information.
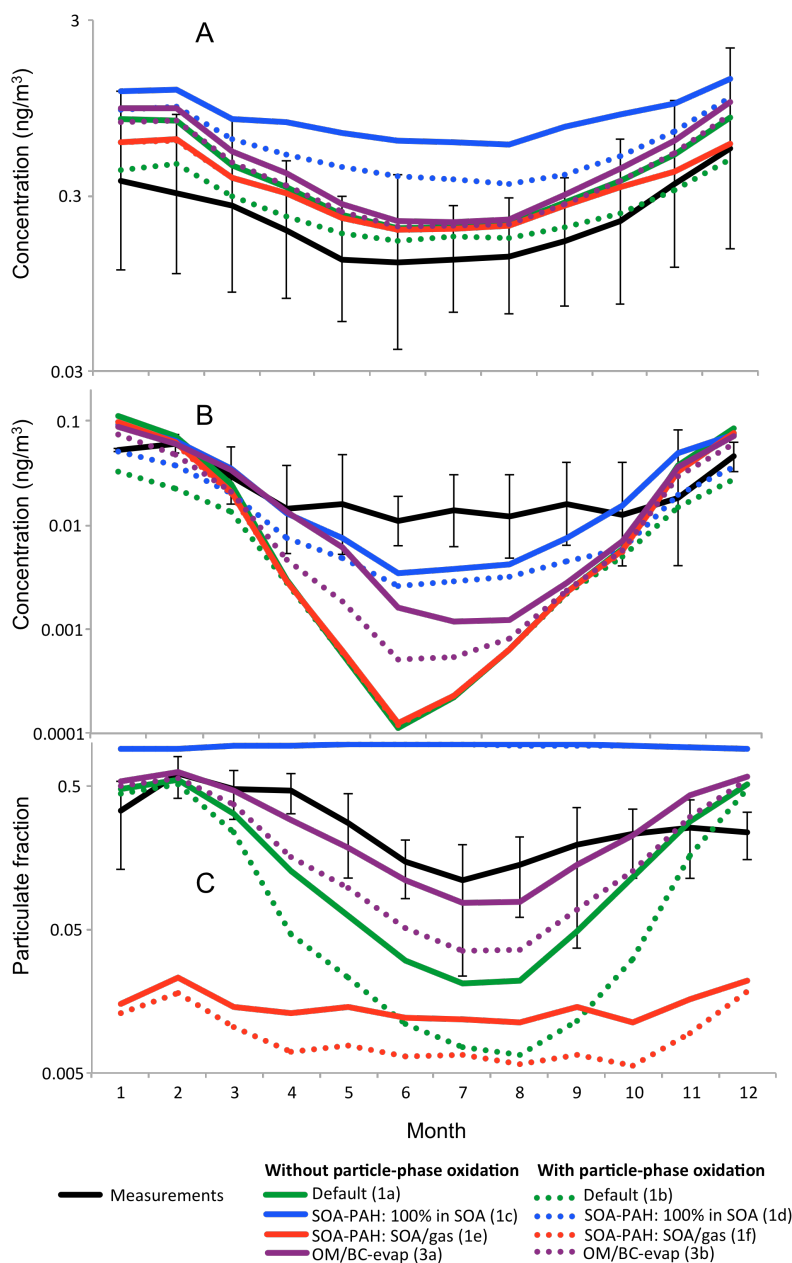
Figures

Figure 1. A) Monthly geometric mean nonurban mid-latitude total concentrations; B) monthly geometric mean Arctic total concentrations; and, C) monthly mean particulate fractions. Results shown are from simulations listed under #1 and #3 of Table 1. Results for simulations without particle phase oxidation (solid lines) and with (dotted lines) are shown. Measured data are for sites in Table S2 for 2006-2008. Error bars are ± 1 standard deviation of monthly means across sites. Numbers/letters in parentheses correspond to simulation labels from Table 1.

702

Legend:
- Measurements
- Default (1a)
- SOA-PAH: SOA/gas (1e)
- SOA-PAH: SOA/gas with [OM+BC] instead of [SOA] (2c)

703

Figure 2. A) Monthly geometric mean nonurban mid-latitude total concentrations; B) monthly geometric mean Arctic total concentrations; and, C) monthly mean particulate fractions for sensitivity simulations. Simulations did not include particle-phase oxidation, and SOA-PAH model simulations were conducted with 20% evaporation by 24 hours. Numbers/letters in parentheses correspond to simulation labels from Table 1.

Assessing the influence of secondary organic aerosols on long-range atmospheric PAH transport – Supporting Information

C. L. Friedman[1], J.R. Pierce[2], and N. E. Selin[3]

[1] Center for Global Change Science and Leading Technology and Policy Initiative, Massachusetts Institute of Technology, Cambridge, Massachusetts

[2] Department of Atmospheric Science, Colorado State University, Fort Collins, Colorado

[3] Engineering Systems Division and Department of Earth, Atmospheric, and Planetary Science, Massachusetts Institute of Technology, Cambridge, Massachusetts

Correspondence to: C. L. Friedman (clf@mit.edu)

Parameter	Description	Value for PYR	Ref
log K_{OA}	Octanol-air partition coefficient	8.86	a
log K_{BC}	Black carbon-air partition coefficient	11.0	b
log K_{AW}	Air-water partition coefficient	-3.27	a
$\Delta_{OA}H$ (kJ/mol)	Enthalpy of phase transfer from gas phase to OC	-87	c
$\Delta_{BC}H$ (kJ/mol)	Enthalpy of phase transfer from gas phase to BC	-87	c
$\Delta_{AW}H$ (kJ/mol)	Enthalpy of phase transfer from water to air	43	c
k_{OH} (cm^3/molec/s)	Reaction rate constant for gas phase oxidation by OH	5.00e-11	d
A (s^{-1})	Kinetic parameter for particle phase oxidation by O_3	7e-4	e
B (molec/cm^3)	Kinetic parameter for particle phase oxidation by O_3	3e15	e
ρ_{oct} (kg/m^3)	Density of octanol	820	b
ρ_{BC} (kg/m^3)	Density of BC	1000	b
τ_{OCBC} (d)	Lifetime of hydrophobic OC and BC before converting to hydrophilic	1.15	f
k_{EVAP80} (s^{-1})	Evaporation rate for 80% PAH remaining on SOA after 24 hours	2.6e-6	g
k_{EVAP50} (s^{-1})	Evaporation rate for 50% PAH remaining on SOA after 24 hours	8.1e-6	g
k_{NO3} (cm^3/molec/s)	Reaction rate constant for particle phase oxidation by NO_3	6.4e-12	h

Table S1. Pyrene physicochemical constants used in the model. References: (a) Ma et al., 2010[1]; (b) Lohmann and Lammel, 2004[2]; (c) Schwarzenbach et al., 2003[3]; (d) U.S. EPA Episuite software[4]; (e) Kahan et al., 2006[5]; (f) Park et al., 2003[6]; (g) deduced from Zelenyuk et al., 2012[7]; (h) Liu et al., 2012[8].

Latitude	Longitude	Station	Observation years	Ref
82	-62	Alert, Canada	2006-2008	1
80	12	Spitsbergen/Zeppelinfjell, Norway	2006-2008	2
68	24	Pallas/Matorova, Finland	2006-2007	2
60	17	Aspvreten, Sweden	2006-2008	2
58	8	Birkenes, Norway	2006, 2008	2
57	12	Rao, Sweden	2006-2008	2
55	8	Westerland, Germany	2006-2008	2
54	13	Zingst, Germany	2006-2008	2
54	-1	High Muffles, Great Britain	2006-2007	2
51	11	Schmucke, Germany	2006-2008	2
50	15	Kosetice, Czech Republic	2006-2008	2
48	8	Schauinsland, Germany	2006-2008	2
47	-88	Eagle Harbor, MI, USA†	2006-2007	3
45	-86	Sleeping Bear Dunes, MI, USA†	2006-2007	3
43	-5	Niembro, Spain	2006	2
43	*-79*	*Sturgeon Point, NY, USA†*	*2006-2007*	*3*
42	-88	Chicago, IL, USA†§	2006-2007	3
41	*-82*	*Cleveland, OH, USA†§*	*2006-2007*	*3*

Table S2. Northern hemisphere measurement stations used to evaluate simulated pyrene concentrations against observed. †Gas-particle ratios provided by reference and used to evaluate simulated gas-particle ratios. §Site considered urban and/or highly impacted by local sources and not used to evaluate background concentrations. Sites > 66°N are considered Arctic. Observations formatted similarly (e.g., bold or italics) occurred within the same GEOS-Chem grid box and were averaged. References: (1) Northern Contaminants Program and Environment Canada; (2) Cooperative Programme for Monitoring and Evaluation of Long-range Transmissions of Air Pollutants (EMEP); (3) Integrated Atmospheric Deposition Network (IADN). Data from reference 3 was provided prior to a routine QA/QC procedure.

Simulation	Particle Phase Oxidation?	Slope of Best Linear Fit	Intercept of Best Linear Fit	Correlation Coefficient (r)	Log Mean Bias
1a: Default	No	1.05	0.14	0.68	0.16
1b: Default	Yes	0.65	0.10	0.65	-0.08
1c: SOA-PAH, 100% in SOA	No	1.91	0.29	0.70	0.42
1d: SOA-PAH, 100% in SOA	Yes	1.45	0.18	0.69	0.23
1e: SOA-PAH, SOA/gas	No	0.79	0.13	0.66	0.09
1f: SOA-PAH, SOA/gas	Yes	0.79	0.13	0.66	0.09
3a: OM/BC-evap	No	1.23	0.16	0.69	0.21
3b: OM/BC-evap	Yes	1.10	0.14	0.68	0.14

Table S3. Linear best-fit slopes, intercepts, and correlation coefficients for mean annual model-observation comparisons shown in Figure S4. The log mean bias (LMB) is also presented, and is given as

$$LMB = \frac{\sum_i (\log_{10}(S_i) - \log_{10}(O_i))}{N}$$

where S_i and O_i are simulated and observed pyrene concentrations at each observation location, i, and N is the number of observation locations.
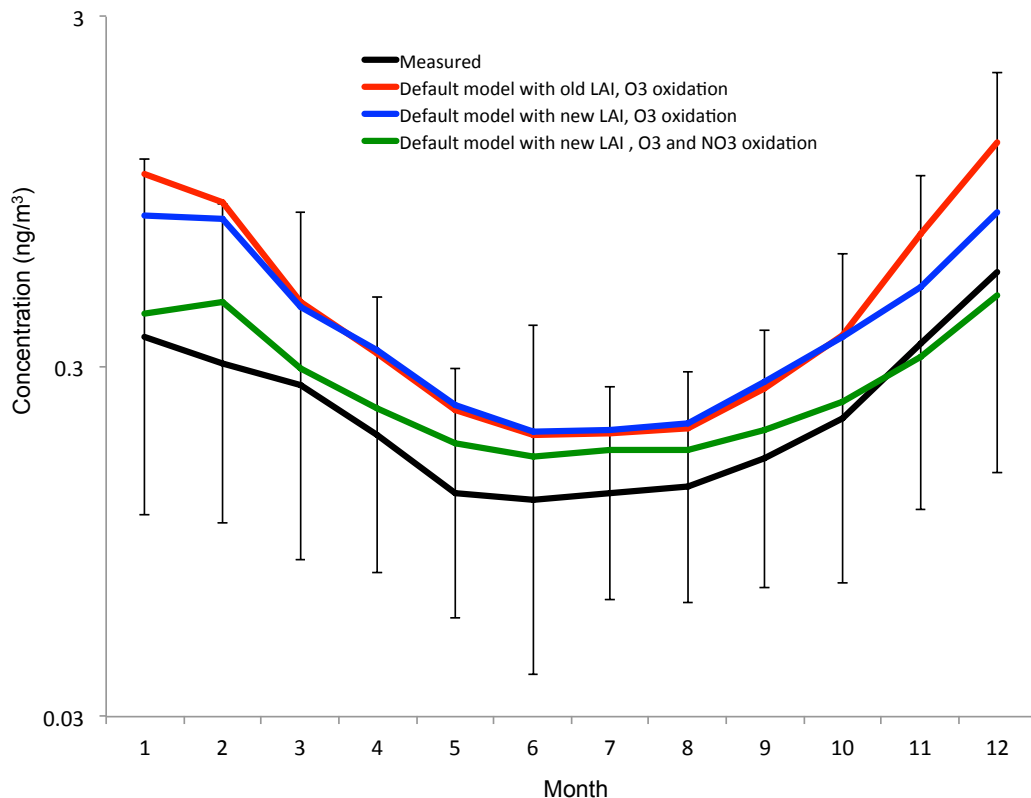
Figure S1. Comparison of pyrene concentrations (mean of 2006-2008) simulated with a previously published version of the model to the version in the present study, which uses two new processes. First, the present Leaf Area Index (LAI) dataset is derived from the Moderate Resolution Imaging Spectroradiometer (MODIS) of NASA's Terra satellite, versus the NOAA Advanced Very High Resolution Radiometer (AVHRR) satellite as was done previously. This is because the MODIS LAI dataset has greater global coverage, includes data specific to model years used here, and is the default dataset for the NO_x-Ox-hydrocarbon-aerosol GEOS-Chem model used for generating all particle and oxidant fields. Second, we include particle-phase oxidation by NO_3 in the present model, compared to particle-phase oxidation only by O_3 in the previous version.
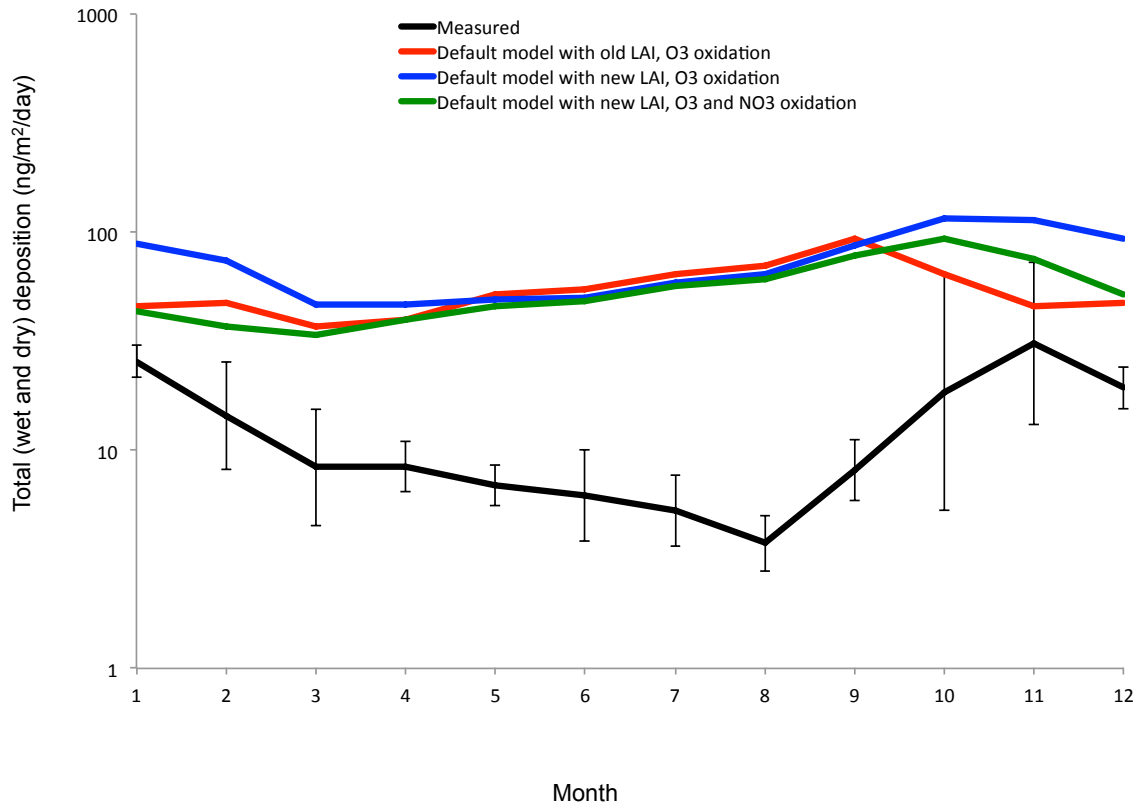
Figure S2. Same figure as S1 but showing the sum of wet and dry pyrene deposition rather than concentration (mean of 2006-2008). Wet and dry deposition are evaluated only for stations routinely reporting it (those from Sweden and Finland listed in Table S2).
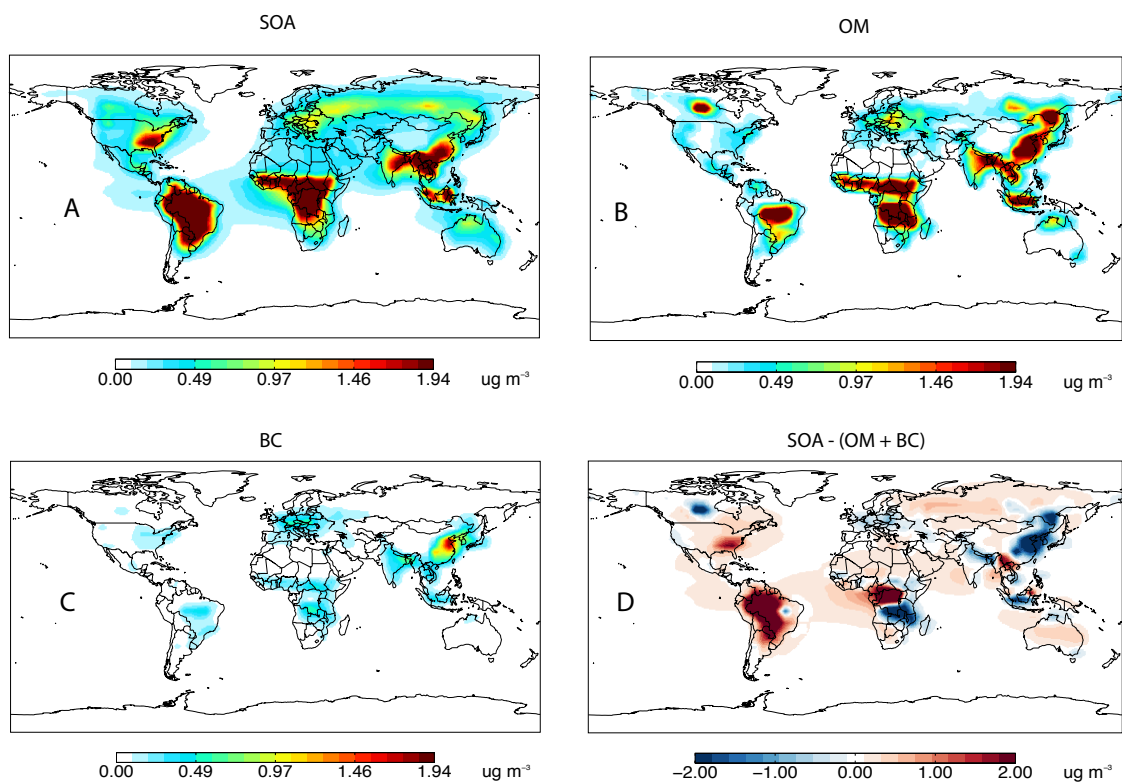
Figure S3. Surface concentrations (μg m^{-3}) of (A) SOA, (B) primary hydrophobic OM, and (C) primary hydrophobic BC, as simulated by GEOS-Chem (mean of 2006-2008). Also shown is the difference between SOA and primary aerosol concentrations (D).
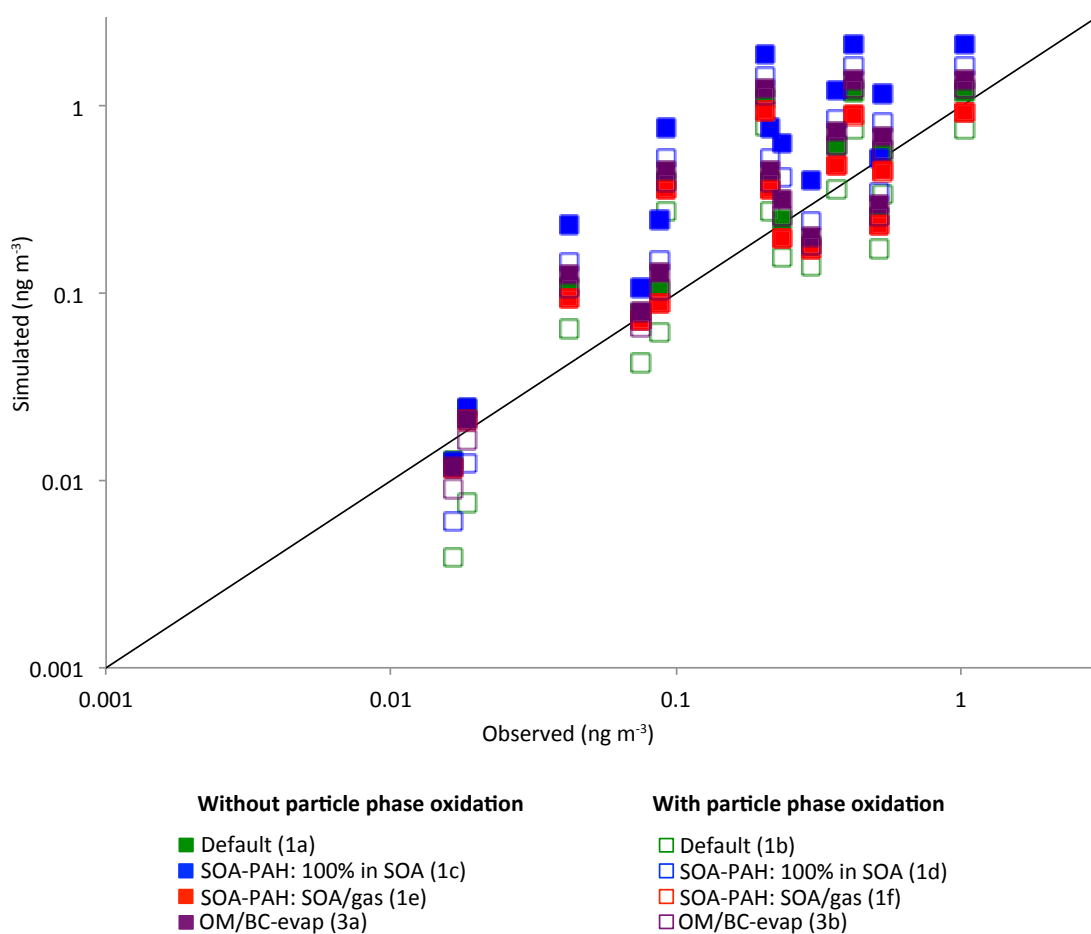
Figure S4. Simulated (2006-2008) versus observed annual mean total pyrene concentrations from sites in Table S2. Numbers/letters in parantheses are simulation labels from Table 1 in the main text.
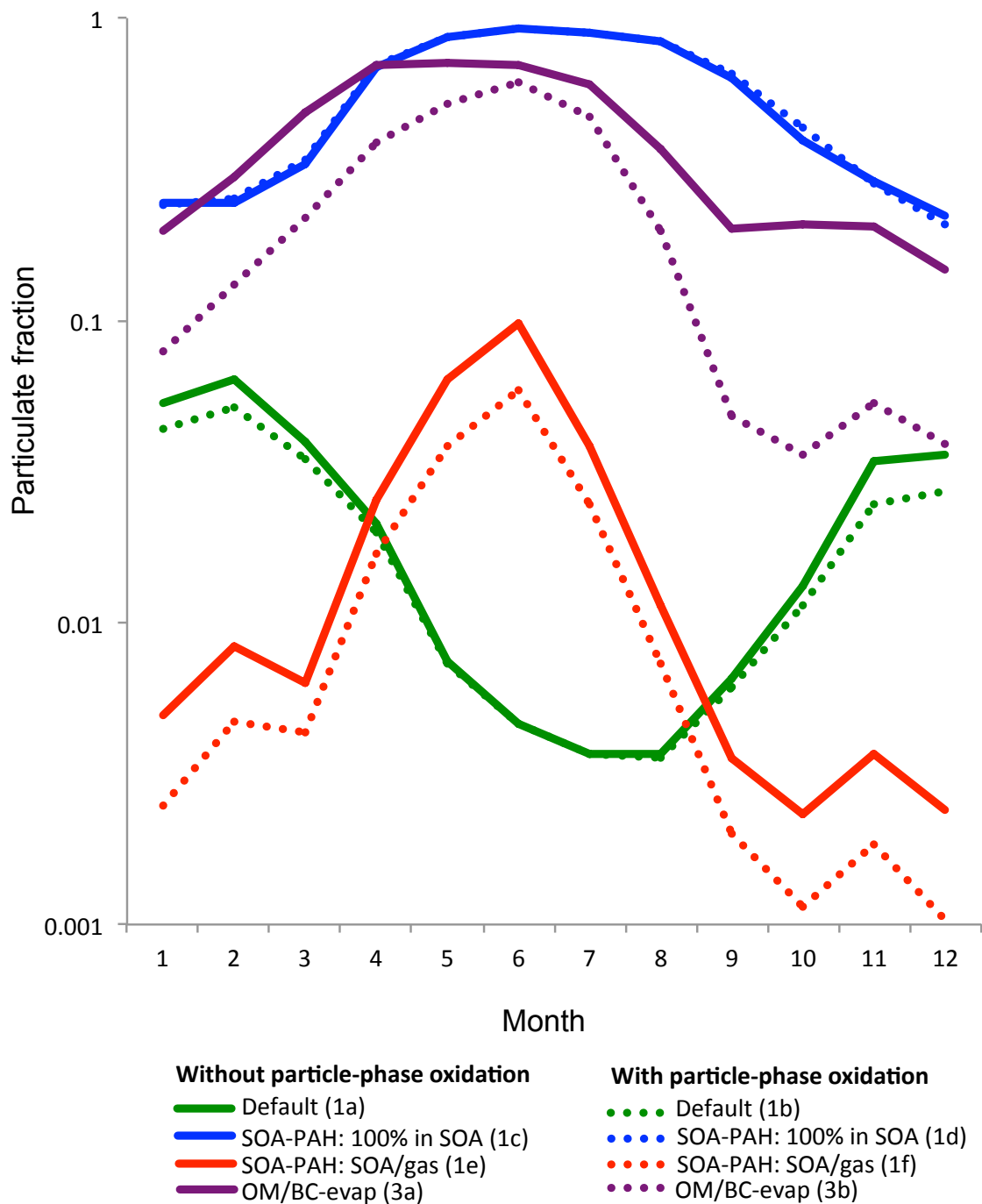
Figure S5. Simulated pyrene particulate fraction in the Arctic. Simulated values are means from GEOS-Chem grid boxes corresponding to Arctic observation stations (see Table S2). Numbers/letters in parentheses correspond to simulation labels in Table 1 in the main text.
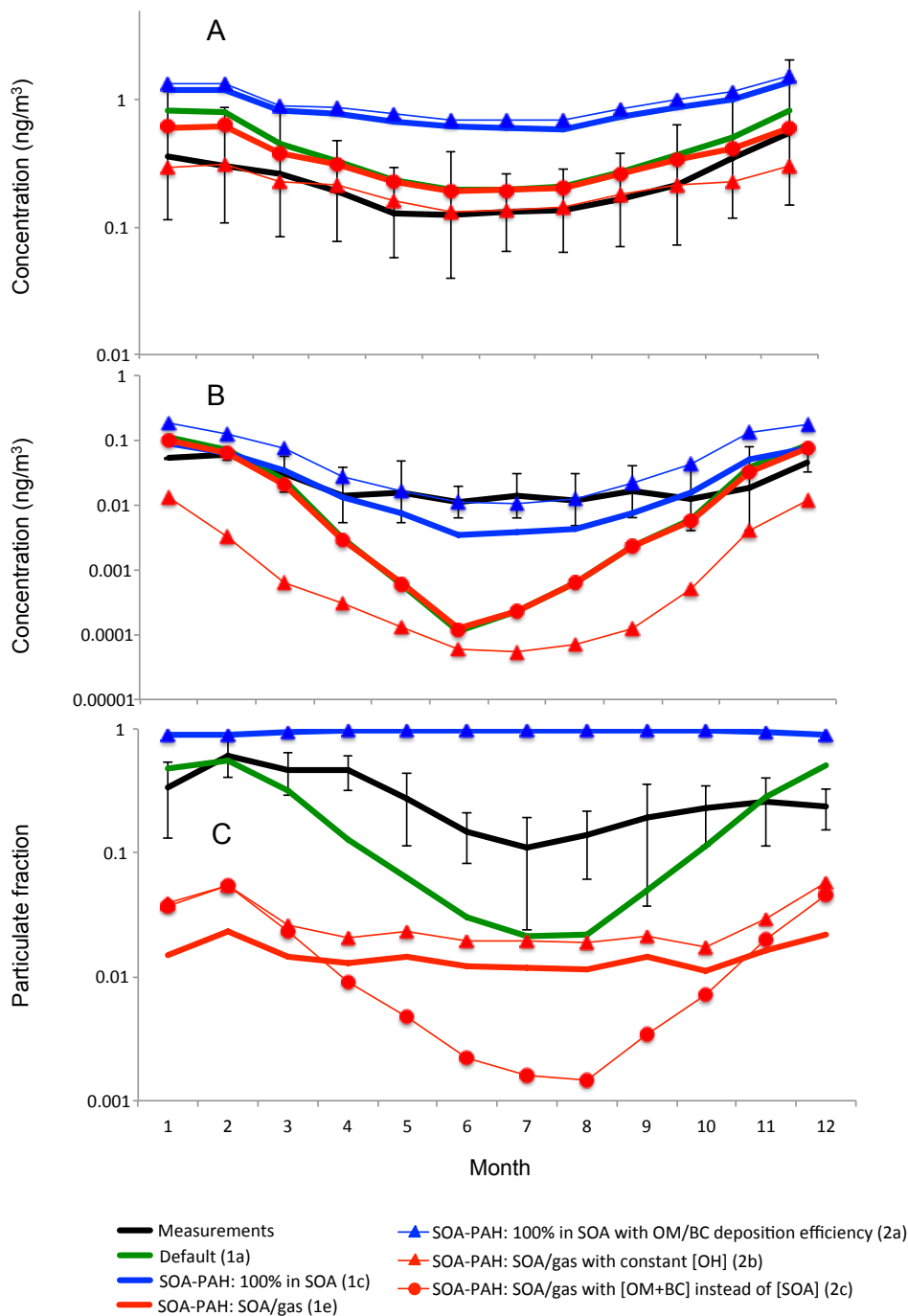
Figure S6. A) Monthly geometric mean nonurban mid-latitude total concentrations; B) monthly geometric mean Arctic total concentrations; and, C) monthly mean particulate fractions for sensitivity simulations. Simulations did not include particle-phase oxidation,

and SOA-PAH model simulations were conducted with 20% evaporation by 24 hours. Numbers/letters in parentheses correspond to simulation labels from Table 1.

Figure S4 shows results of our three sensitivity simulations to test the influence of wet deposition efficiency, OH concentrations, and spatiotemporal aerosol distribution, respectively (simulations 2a-2c, Table 1) compared with observations (mid-latitude means in A, Arctic means in B, and particulate fraction in C). Also shown for comparison are default and SOA-PAH configuration results for simulations without particle-phase oxidation (i.e., simulations 1a, 1c, and 1e; solid green, blue, and red lines from Fig. 1).

Wet deposition efficiency changes have little impact on overall results (blue line with triangles). Replacing SOA wet deposition efficiency with that of primary OM/BC increases the high bias in simulated concentrations. Mid-latitude concentrations increase by 13% (Fig. S4A) and Arctic concentrations increase by 2.3x (Fig. S4B). Phase distribution does not change (Fig. S4C); particle fractions are still considerably overestimated.

Applying a constant OH concentration (red lines with triangles) increases gas-phase oxidation (+11% increase in the annual budget), leading to 1.7x lower total mid-latitude concentrations (Fig. S4A), 8.9x lower Arctic concentrations (Fig. S4B), and 1.9x higher particulate fractions (Fig. S4C). Though this generally improves model-measurement agreement in the mid-latitudes, the particle phase is still largely underestimated compared to observations, as are Arctic concentrations.

Results for substituting primary OM/BC concentrations for SOA (red line with circles) are discussed in the main text.

Literature Cited

1.   Ma, Y.-G.; Lei, Y.; Xiao, H.; Wania, F.; Wang, W.-H. Critical review and recommended values for the physical-chemical property data of 15 polycyclic aromatic hydrocarbons at 25 C. *J. Chem. Eng. Data* **2010,** *55*, 819-825.

2.   Lohmann, R.; Lammel, G. Adsorptive and absorptive contributions to the gas-particle partitioning of polycyclic aromatic hydrocarbons: State of knowledge and recommended parametrization for modeling. *Environ. Sci. Technol.* **2004,** *38*, 3793-3803.

3.   Schwarzenbach, R. P.; Gschwend, P. M.; Imboden, D. M., *Environmental Organic Chemistry*. 2nd ed.; 2003.

4.   EPA, U. S. Estimation Programs Interface Suite for Microsoft Windows, v 4.10. United States Environmental Protection Agency, Washington DC, USA. **2011**.

5.   Kahan, T. F.; Kwamena, N.-O. A.; Donaldson, D. J. Heterogeneous ozonation kinetics of polycyclic aromatic hydrocarbons on organic films. *Atmos. Environ.* **2006,** *40*, 3448-3459.

6.   Park, R. J.; Jacob, D. J.; Chin, M.; Martin, R. V. Sources of carbonaceous aerosols over the United States and implications for natural visibility. *J. Geophys. Res.* **2003,** *108(D12)*, 4355.

7.   Zelenyuk, A.; Imre, D.; Beranek, J.; Abramson, E. H.; Wilson, J.; Shrivastava, M. Synergy between secondary organic aerosols and long-range transport of polycyclic aromatic hydrocarbons. *Environ. Sci. Technol.* **2012,** *46*, 12459-12466.

8.   Liu, C.; Zhang, P.; Yang, B.; Wang, Y. X.; Shu, J. Kinetic studies of heterogeneous reactions of polycyclic aromatic hydrocarbon aerosols with NO_3 radicals. *Environ. Sci. Technol.* **2012,** *46*, 7575-7580.